GSA Data Repository 2020185

King, C., Hall, B., Hillebrand, T., and Stone, J., 2020, Delayed maximum and recession of an East Antarctic outlet glacier: Geology, v. 48, https://doi.org/10.1130/G47297.1

Supplemental Material

DETAILED GLACIAL GEOMORPHOLOGY

Drift on Lake Wellman and entrained in Hatherton Glacier

The perennial ice cover of Lake Wellman displays numerous, ice-cored debris mounds, the most prominent of which is a large, blocky sandstone boulder resting atop an ice-cored talus skirt (Fig. S1). Close inspection of the two largest, conical debris mounds revealed gravel-sized or larger, angular sediment particles. The most prominent feature, a thick, hummocky ice-cored landform with multiple cross-cutting ridges and several meters of relief, is located between Hatherton Glacier and the lake. In addition, several similar but smaller mounds, as well as a variety of erratics, are melting out of Hatherton Glacier. Most erratics exhibit heavy staining, although there are also a limited number of moulded, faceted, and fresh clasts (Fig. S1). These latter erratics are almost entirely granite, diorite or sandstone.

Hatherton drift

Hatherton drift extends ~1.8-2.0 km into the main valley from the present-day glacier terminus (860 m elevation) to a maximum observed elevation of 1000 m, although the limit is poorly defined (Figs. S1, S2). In general, the drift can be separated into two parts: 1) a thick deposit, ice-cored in places, immediately adjacent to the glacier on the south side of the field area, and 2) thin deposits outboard of Lake Wellman. In the former location, there are ice-cored conical mounds, similar to those on the lake. The most prominent feature is a sharp, discontinuous ridge (4 m relief), named Moraine 1 by Storey et al. (2010), that extends oblique to the present-day margin for 0.8 km and, because of its odd orientation, is not thought to be an ice-marginal feature. These thick deposits are matrix-supported with silty, gravelly sediment and

typically heavily weathered boulders. Some erratics exhibit staining over striations, however, there are also rare fresh, moulded and striated clasts.

In contrast to the area south of Lake Wellman, Hatherton drift distal to the lake is a thin sheet, typically only one boulder thick. Constructional landforms are limited to ice-contact terraces on a ridge separating the northern two lobes of the lake ice and to hummocky ridges, including one (Moraine D) located ~100 m above the present-day lake elevation. The drift commonly is composed of highly weathered erratics, particularly heavily stained dolerites, but also sandstones and a few granites. Both types of Hatherton drift contain abundant deposits of sub-fossil cyanobacteria.

Britannia I drift

Britannia I deposits occur outboard of Hatherton drift and extend as much as 3.3 km from the glacier terminus along the main valley axis (Figs. S1, S2). Here, the drift limit at 1130 m elevation (~270 m above present-day ice level at Lake Wellman) is marked by a distinct, laterally extensive ridge of openwork gravel to boulders (11 m of relief), termed Moraine 2 by Storey et al. (2010) (Figs. S1, S2). To the north and south of the moraine, the limit rises in elevation. To the north, the drift edge skirts the valley and then fades into colluvium; to the south, it can be traced nearly continuously to the north side of the saddle leading to Darwin Depression, a closed basin in the upper part of the westernmost valley in the Lake Wellman region. South of the saddle, the limit is visible as an ice-cored drift edge, which extends to the valley mouth and along the plateau adjacent to Hatherton Glacier between Lake Wellman and Lake Hendy. The maximum measured elevation of Britannia I drift in our field area occurs here

at ~1300 m. Overall, Britannia I drift is thin and commonly exposes windows of highly weathered drift from previous glaciations.

Britannia I drift displays numerous, laterally extensive recessional moraines. Moraines A, B, and C occur inboard of the limit at 1090, 1065, and 1030 m elevation, respectively, along the main axis of the valley (Fig. S2). These ridges are continuous for as much as ~0.9 km and typically are sharp-crested, narrow features with less than two meters of relief, although Moraine B has more than four meters of relief in places. Moraine A is marked only by an increase in boulder density. Several closely spaced moraine crests also occur near the lip of the Darwin Depression.

In general, Britannia I drift is composed of stained, angular clasts with only rare fresh erratics (Fig. S1). At the limit in the main valley, erratics consist of red-stained, slightly angular dolerite and brown-stained sandstone, with rare granite. Some sandstone clasts exhibit signs of exfoliation. However, there are sufficient unweathered or slightly weathered clasts to give the deposits a distinct gray color at the limit, compared to outboard deposits. Moreover, in contrast with the older drifts, abundant subfossil cyanobacteria are associated with Britannia I deposits. Cyanobacteria occur beneath boulders set into the surface of the drift.

Britannia I drift in Darwin Depression differs in morphology from that in the main valley. The eastern half of the basin contains hummocky, strongly weathered drift with fractured, heavily stained, generally rounded erratics. To the west, the hummocks give way to kame and kettle topography. Most kames are composed of loose, gravelly diamicton with a surface pavement of cobbles and gravel. The major landform on the basin floor is a sharp-crested, sinuous ridge (3-4 m relief) that trends east-west. Its hummocky crest suggests it that may be

ice-cored. The ridge is similar in size, shape, orientation and composition to Moraine 1 and contains ~5% moulded, faceted, and striated cobbles, some with staining over the striations.

Because the saddle separating Darwin Depression from the main valley is at only 1020 m elevation, Britannia I ice likely was thick enough to overtop the sill and flow into the basin. We base this inference on the fact that Britannia I drift extends to 1130 m elevation in the main valley, 2.5 km north of the lake, and the limit rises toward Darwin Depression. In addition, degraded lateral moraines associated with Britannia I drift slope down into the basin from the saddle, indicating ice flow from the main valley. Hummocky, kame and kettle topography that is prevalent in the basin can be explained by stagnation of an ice mass that became separated from Hatherton Glacier during recession. An alternate interpretation for the hummocky topography is that it was formed by a lake-ice conveyor (Hendy et al., 2000).

Overall, our mapped Britannia I highstand of Hatherton Glacier closely matches the Britannia limit of Bockheim et al. (1989). However, Bockheim et al. (1989) could not distinguish between Britannia I and the older Britannia II drift in the Lake Wellman region and inferred that their mapped Britannia limit likely represented the Britannia II extent rather than Britannia I as we propose here. Based on our more detailed mapping, on comparison with other sites alongside Hatherton Glacier, and on weathering characteristics, we were able to identify a Britannia II drift limit outboard of the Britannia I limit. The Britannia II limit is marked by a distinct clast-rich ridge at ~1245 m elevation in the main valley <0.3 km distal to the Britannia I drift edge. The ridge crest is sharp (2 m relief), covered with large boulders, continuous for ~1.0 km, and composed of primarily slightly stained, exfoliating sandstone. Britannia II drift has been shown elsewhere along Hatherton Glacier to date to the penultimate glaciation (Joy et al., 2014). As this age is consistent with the observed degree of weathering, we adopt that age here

for Britannia II drift. Deposits distal to Britannia II are more strongly weathered and relate to older Danum and Isca drifts (Bockheim et al., 1989). We did not find cyanobacterial mats associated with any drift older than Britannia I.

Glaciolacustrine Deposits

The locations of former lakes associated with Britannia and Hatherton drifts can be identified in many cases by surface texture and morphology. Typically, such sites show erratics slightly set into a smooth sandy, gravely surface. In some locations, tightly interlocking cobbles and boulders have been pressed into flat pavement surfaces (Fig. S2, S3). *In situ* sub-fossil cyanobacterial mats are preserved commonly in sorted silt, sand, and gravel sediment beneath and around clasts. In addition, relict shorelines are etched into Britannia I drift in several places (Fig. S3). Most of these abandoned lake deposits and landforms occur on surfaces that slope down toward the present-day ice margin, and therefore a thicker Hatherton Glacier must have existed in order to dam the water to these levels.

RADIOCARBON RESULTS AND INTERPRETATION

Forty-five radiocarbon dates of sub-fossil cyanobacteria mats were collected along two primary transects, one between Lake Wellman and the Darwin Depression and the second along the main valley axis (Transects A and B, respectively; Table S1, Fig. S2). Eleven samples along Transect A yielded ages ranging from ~8400-6500 yr BP. Three samples from Darwin Depression – two from the sinuous ridge crest and one from the basin floor – range from 8110 ± 80 to 8400 ± 50 yr BP. These samples require an ice-dammed lake capable of spilling over the saddle at 1020 m elevation. One sample within the moraine complex on the saddle above the

depression dates to 7880 ± 150 yr BP (OS-111893). A prominent lake basin with relict shorelines occurs immediately proximal to these moraines and produced five ages of 7760 ± 80 to 8670 ± 120 yr BP, with four clustering tightly between 7760 ± 80 and 7870 ± 80 yr BP. We consider the oldest age to be an outlier. This shoreline grades into the sill leading to the Darwin Depression and may reflect a time when water level had just dropped below the sill. A sample collected less than 20 m elevation below these shorelines produced an age of 6570 ± 80 yr BP (OS-111169). Cyanobacteria collected along the transect at ~50 m above Lake Wellman in a basin west of Moraine 1 dated to 3310 ± 70 yr BP (OS-110172).

We dated 33 samples along Transect B in the main valley (Fig. S2, Table S1). Three samples in a small basin dammed against the distal slope of Moraine 2 at the Britannia I limit produced a mean age of 9520 ± 50 yr BP, which we take to be the best estimate of the timing of the local glacial maximum. Six samples immediately proximal to Moraine 2 range from 8690 ± 100 to 11,220 ± 70 yr BP. Another sample, proximal to the Britannia I limit in the northeast region of the main valley, yielded an age of 8370 ± 40 yr BP. The remainder of the samples associated with Britannia I drift occur at lower elevations and fall between ~13,000 yr BP and 6000 yr BP. Two samples distal to Moraine A are 10,350 ± 100 and 10,320 ± 90 yr BP. Between Moraines A and B, three samples in the northern part of the valley range from 7250 ± 80 and 8250 ± 230 yr BP in age. Farther south, two samples between the same two moraines are 12,980 ± 140 and 12,620 ± 100 yr BP. At lower elevation distal to Moraine C, four samples date from 6120 ± 180 to 6440 ± 50 yr BP. Two samples from the crest of the moraine itself cluster tightly between 6360 ± 50 and 6530 ± 210 yr BP, and one sample immediately proximal to the moraine dates to 6440 ± 140 yr BP (OS-111899). Eleven radiocarbon samples at even lower elevations in Hatherton drift range from ~5960-2500 yr BP. The two most distal samples within Hatherton

drift are 5960 ± 40 and 5300 ± 20 yr BP (OS-111163 and OS-111164). Six samples bracketing the lower-elevation Moraine D range from 4850 ± 70 to 4360 ± 70 yr BP. The lowest sample, collected at ~20 m above present-day Lake Wellman, produced an age of 2810 ± 40 yr BP (OS-117593). We did not collect samples closer to the lake due to snow cover.

We propose the following conceptual model for the origin of the cyanobacteria mats in glaciolacustrine deposits high above the present-day lake (Fig. S4). Because of the valley slope, most lakes in Lake Wellman valley must be dammed against the margin of Hatherton Glacier. Thus, the position and elevation of the lakes are controlled by the extent and elevation of the glacier. As the glacier advances up the slope, it overrides deposits from its former lakes. We suspect that rare deposits formed during the advance were preserved close to the Britannia drift limit and are reflected by a cluster of anomalously old ages in the main valley that decrease in age with increasing elevation. Most of our samples, however, reflect recession of Hatherton Glacier down the slope toward its present-day position. As the glacier receded, the lake followed the glacier (Fig. S4), leading the cyanobacterial mats to display the decreasing radiocarbon ages with decreasing elevation that characterizes our dataset. Moreover, each sample of cyanobacteria affords information on 1) minimum ice level needed to dam the water body and 2) minimum age for deglaciation of the specific site of the sample.

Small vs. Large Lakes

We interpret our data as indicating a series of small, short-lived ice-marginal lakes, rather than as fluctuations of a single long-lived large lake dammed by a distant ice margin. Although it is possible that a single large lake could have filled the valley at some time in the past, we do not see evidence of this. As benthic mats can live at a range of water depths, we would expect to see

numerous radiocarbon dates of the same age at a variety of locations and elevations, if a large lake filled the valley. Cyanobacteria of different ages would be in close spatial juxtaposition. Instead, the radiocarbon ages show a strong pattern of decreasing age with decreasing elevation, consistent with small ice-dammed lakes following a retreating ice margin downslope.

In our opinion, another compelling argument in favor of small lakes closely associated with the ice margin rather than a single large lake is the fact that the cyanobacterial mats are only associated with Britannia I and Hatherton drifts. It is highly unlikely that a large lake dammed by a distant ice margin would coincidentally end exactly at the Britannia I limit.

COSMOGENIC NUCLIDE ANALYSES AND EXPOSURE AGES

Cosmogenic ^{10}Be and ^{26}Al analyses of samples analyzed for this study are given in Tables S2 and S3. Exposure ages are calculated with an online calculator (http://hess.ess.washington.edu) using the default CRONUS calibration data set (Borchers et al., 2016; Balco et al., 2008).

Samples for exposure dating were collected during the 2013-14 field season and come from a mix of kilogram-size cobbles and larger boulders. Most are from granite erratics, a rock type that does not crop out in the glacier catchment upstream. We collected from rocks showing patches of glacial smoothing, blunted edges, or other evidence of glacial transport, confirming that there has been minimal erosion since deposition. We did not sample from lee slopes or rocks in the lee of larger boulders, to avoid the possibility of cover by drift snow.

When sampling in Antarctica, we normally target isolated erratics perched on bedrock or on ancient, compacted, geomorphically-stable surfaces. We typically avoid moraines, which are commonly ice-cored and show obvious evidence of collapse and accompanying disturbance.

This was not always possible at Lake Wellman, where there are few bedrock outcrops below the Britannia-I depositional limit, and much of the valley floor is covered with comparatively thick recessional drift. Instead, where possible, we sampled from the edges of discontinuous patches of Britannia I and Hatherton drifts, where these deposits were thin enough to reveal underlying, older surfaces, and targeted perched rocks and boulders undisturbed since deposition. In such cases, we compared the degree of weathering on the top and bottom of the rocks to confirm that they had not been overturned. Despite these precautions, 4 of the 7 samples from Britannia I recessional deposits gave exposure ages substantially older than the radiocarbon ages of nearby cyanobacteria mats, confirming that the majority of clasts in this deposit are recycled (*cf.* Storey et al., 2010). Lacking other material to date the maximum Britannia I advance, we also sampled from the moraine that marks the Britannia I limit at two sites, both west and northwest of Lake Wellman (Fig. S2). This moraine was originally ice-cored (and remains so in places), and rocks at the crest may have rotated as it collapsed. We therefore targeted cobble-sized rocks which would receive the same cosmic-ray dose regardless of orientation, as well as rocks with different degrees of weathering on the top and bottom surfaces, indicating a consistent orientation during exposure. Only one of these 8 samples, gave an age close to that of nearby radiocarbon samples (13-HAT-031-LW); the remainder range from ~19-65 ka and appear to be pre-exposed and recycled.

Sample elevations were derived from drift-corrected barometric altimeters, referenced to a network of control points established with a geodetic GPS receiver. Elevation accuracy is typically ± 3-5 m based on repeat measurements during this and other Antarctic field seasons. Topographic shielding of samples was calculated from vertically oriented, full-sky fisheye photographs.

Beryllium and aluminum were extracted and purified for isotopic analysis at the University of Washington Cosmogenic Nuclide Laboratory using established procedures (http://depts.washington.edu/cosmolab/chem.shtml). We crushed and sieved samples and purified quartz from the 250-500 μm or 500-850 μm fractions using a combination of density and surfactant separations and etching with dilute HF (Kohl & Nishiizumi, 1992). After quartz dissolution we purified Be and Al by column chromatography (Ditchburn and Whitehead, 1994). We measured Be isotope ratios at the Lawrence Livermore National Laboratory Center for Accelerator Mass Spectrometry (LLNL-CAMS). Isotope ratios were normalized to the ICN 01-5-4 Be standard, also referred to as KNSTD-3110, assuming a $^{10}Be/^{9}Be$ value of 2.851×10^{-12} (Nishiizumi et al., 2007). Results shown in Table S3 have been corrected for ^{10}Be blanks of ~ 1-2 x 10^4 atoms, less than 1% of the total ^{10}Be measured except in the case of the young sample 13-HAT-049a-LW (7.2 ± 2.2%). We measured Al isotope ratios at PRIME Lab, where Al is analyzed by injecting molecular AlO^- and a gas-filled magnet is used to suppress interference by ^{26}Mg ions. In terms of ions counted, the sensitivity of ^{26}Al measurements is within a factor of two of ^{10}Be measurements at LLNL-CAMS, and final uncertainties of the ^{10}Be and ^{26}Al concentrations are comparable.

Most of the ^{10}Be measurements for this project were made at LLNL-CAMS during 2011-2014. Analyses of UW cathodes containing ICN Be standard material run concurrently with these measurements scattered by significantly more than their reported uncertainties, indicating a source of analytical error not accounted for in the data processing and reporting. To incorporate this additional source of uncertainty, we have increased the error assigned to unknown samples run with the UW standards as described below.

In each accelerator run we analyzed 1-11 cathodes containing 250-270 micrograms of the ICN-01-5-4, ICN-01-5-3 and ICN-01-6-1 reference standards (Nishiizumi et al., 2007) prepared from purchased solutions. These were run openly (not blind) and results processed as unknowns alongside regular samples. Isotope ratios for 65 of these UW-KNSTD standards run in this period ranged from 0.904 ± 0.010 to 1.129 ± 0.010 of their expected values. In all AMS runs UW standard cathodes produced less accurate results than LLNL internal standard cathodes containing the same reference materials. For each run with more than one UW-KNSTD standard analysis we calculated the dispersion and bias of the UW standard cathodes. Reduced χ^2 values ranged from 3.2 to 185; bias of the analyses from -8.3 ± 1.0 % to +5.1 ± 3.4%. The high χ^2 values indicate a source of error in the analysis of UW cathodes not accounted for in their reported uncertainties. We estimate this additional error σ_E for each run as the amount which, when added to the reported errors in quadrature, brings the reduced χ^2 of the UW KNSTD data to 1:

For a set of n UW-KNSTD analyses with measured $^{10}Be/^{9}Be$ ratios $R_{m,i}$, normalized to their standard values R_{std}, and reported errors $\sigma_{m,i}$, the reduced χ^2 value is given by:

$$\chi^2/(n-1) = 1/(n-1)\sum_{i=1}^{n}\frac{(R_{m,i}/R_{std}-1)^2}{(\sigma_{m,i}/R_{std})^2}$$

and the additional error required to bring chi-squared to 1, σ_E, is given by:

$$1 = 1/(n-1)\sum_{i=1}^{n}\frac{(R_{m,i}/R_{std}-1)^2}{(\sigma_{m,i}/R_{std})^2 + {\sigma_E}^2}$$

For AMS ^{10}Be runs in 2011-2014 this additional error ranges from zero up to 9.1%. For the samples in this data set an additional error of 2.2% was applied to 3 of the 17 samples. The remainder were either analyzed in runs with a single UW KNSTD, or in runs in early 2015 in which χ^2/(n-1) of the UW standard analyses was < 1. For the 3 samples assigned additional error, bias in accompanying standard analyses was -0.8 ± 2.8% and has not been corrected.

SUPPLEMENTAL REFERENCES

Balco, G., Stone, J. O., Lifton, N. A., and Dunai, T. J. (2008). A complete and easily accessible means of calculating surface exposure ages or erosion rates from ^{10}Be and ^{26}Al measurements. Quaternary Geochronology, 3, 174-195.

Bockheim, J.G., Wilson, S.C., Denton, G.H., Andersen, B.G., and Stuiver, M., 1989, Late Quaternary ice-surface fluctuations of Hatherton Glacier, Transantarctic Mountains: Quaternary Research, v. 31, p. 229–254.

Borchers, B., Marrero, S., Balco, G., Caffee, M., Goehring, B., Lifton, N., Nishiizumi, K., Phillips, F., Schaefer, J. and Stone, J. (2016). Geological calibration of spallation production rates in the CRONUS-Earth project. Quaternary Geochronology, 31, 188-198.

Ditchburn, R.G. and Whitehead, N.E. (1994). The separation of ^{10}Be from silicates. 3rd Workshop South Pacific Environ. Radioact. Assoc., pp. 4-7.

Hendy, C.H., Sadler, A.J., Denton, G.H., and Hall, B.L., 2000, Proglacial lake-ice conveyors: A new mechanism for deposition of drift in polar environments: Geografiska Annaler Series A, v. 82, p. 249–270.

Joy, K., Fink, D., Storey, B.C., and Atkins, C., 2014, A 2 million year glacial chronology of the Hatherton Glacier, Antarctica and implications for the size of the East Antarctic Ice Sheet at the last glacial maximum: Quaternary Science Reviews, v. 83, p. 46–57.

Kohl, C. P., and Nishiizumi, K. (1992). Chemical isolation of quartz for measurement of in-situ-produced cosmogenic nuclides. Geochimica et Cosmochimica Acta, 56, 3583-3587.

Nishiizumi, K., Imamura, M., Caffee, M. W., Southon, J. R., Finkel, R. C., and McAninch, J. (2007). Absolute calibration of ^{10}Be AMS standards. Nuclear Instruments and Methods in Physics Research Section B: Beam Interactions with Materials and Atoms, 258, 403-413.

Storey, B.C., Fink, D., Hood, D., Joy, K., Schulmeister, J., Riger-Kusk, M, and Stevens, M.I., 2010. Cosmogenic nuclide exposure age constraints on the glacial history of the Lake Wellman area, Darwin Mountains, Antarctica: Antarctic Science, v. 22, p. 603-618.

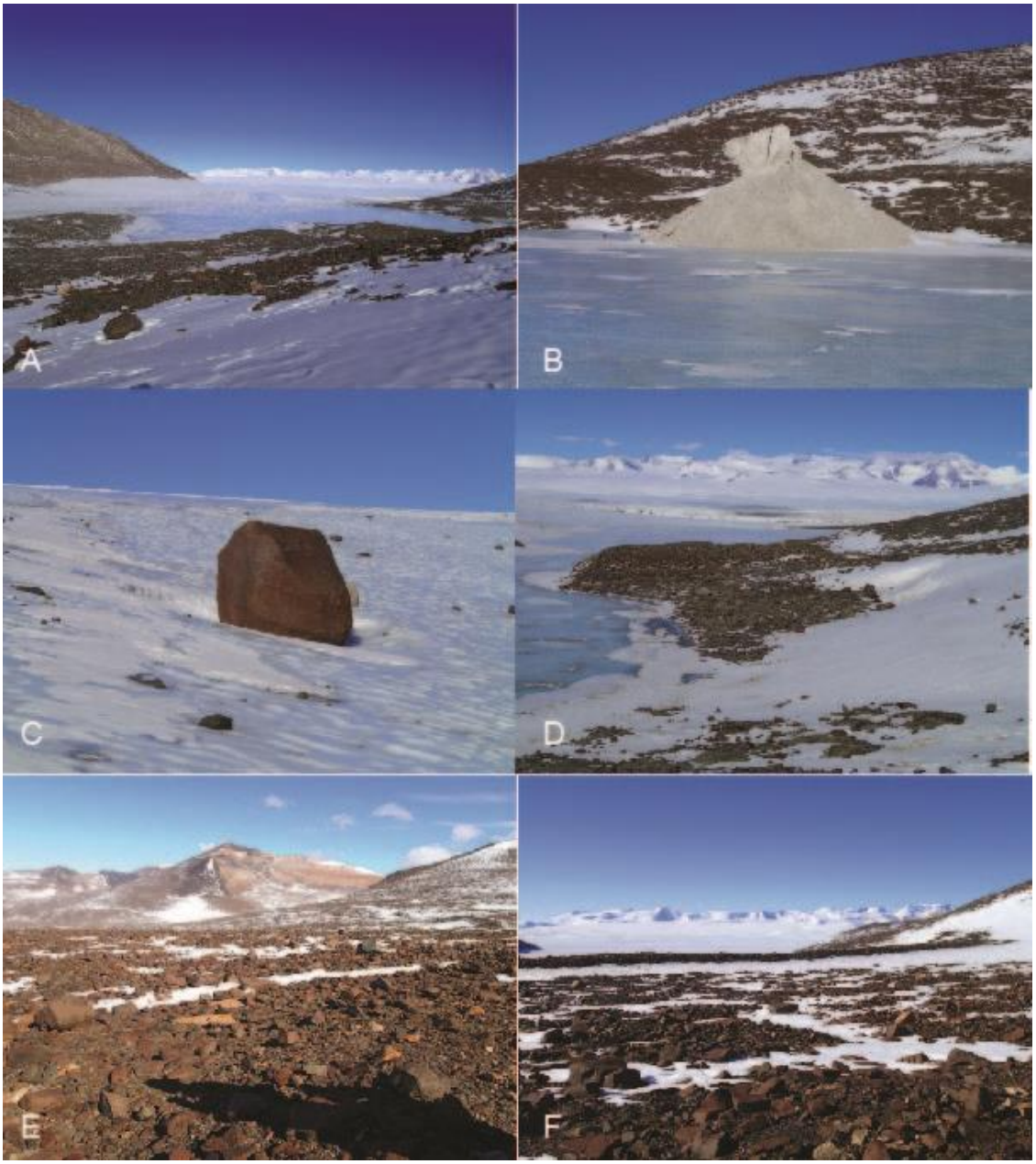

Figure S1. A. View of Lake Wellman and Hatherton Glacier, Transantarctic Mountains. B. Ice-cored debris cone (~6 m high) on the surface of Lake Wellman. C. Weathered dolerite erratic (~1.2 m high) emerging from the present-day glacier. D. Hatherton drift adjacent to Lake Wellman, including Moraine 1. E. Weathered Britannia I drift surface. F. Britannia I drift limit, marked here by a prominent moraine (about half a km long in this photograph). View is of the distal moraine slope toward the east.

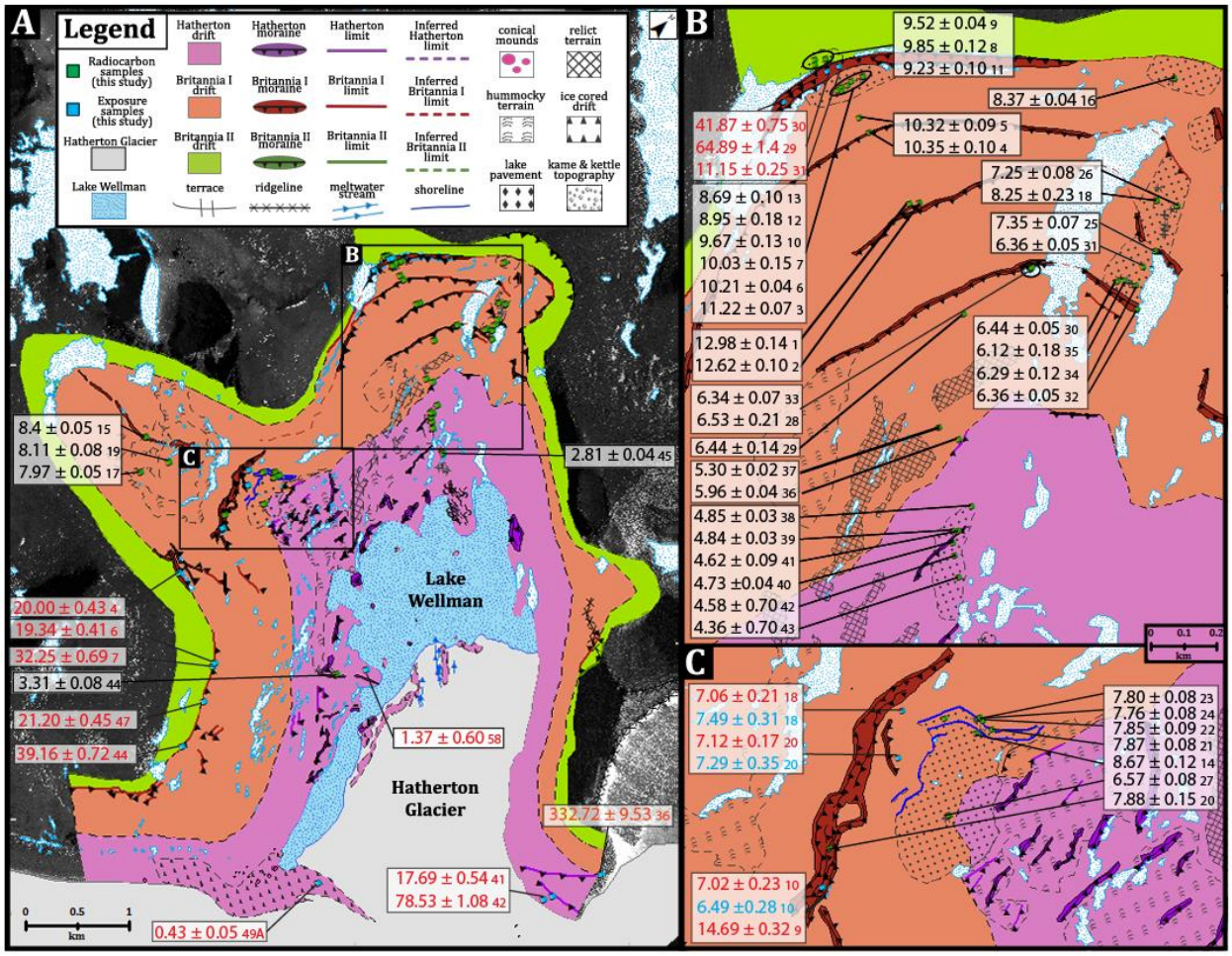

Figure S2. Surficial geomorphology and geochronologic data, Lake Wellman region. Map shows the principal surficial deposits, as well as the radiocarbon (black), ^{10}Be (red) and ^{26}Al (blue) ages in thousands of years. Small numbers following radiocarbon dates are keyed to the first column of Table S1. Similar numbers following the beryllium and aluminum ages can be found in the sample names in Table S2. Boxed letters by moraines denote the informal moraine names.

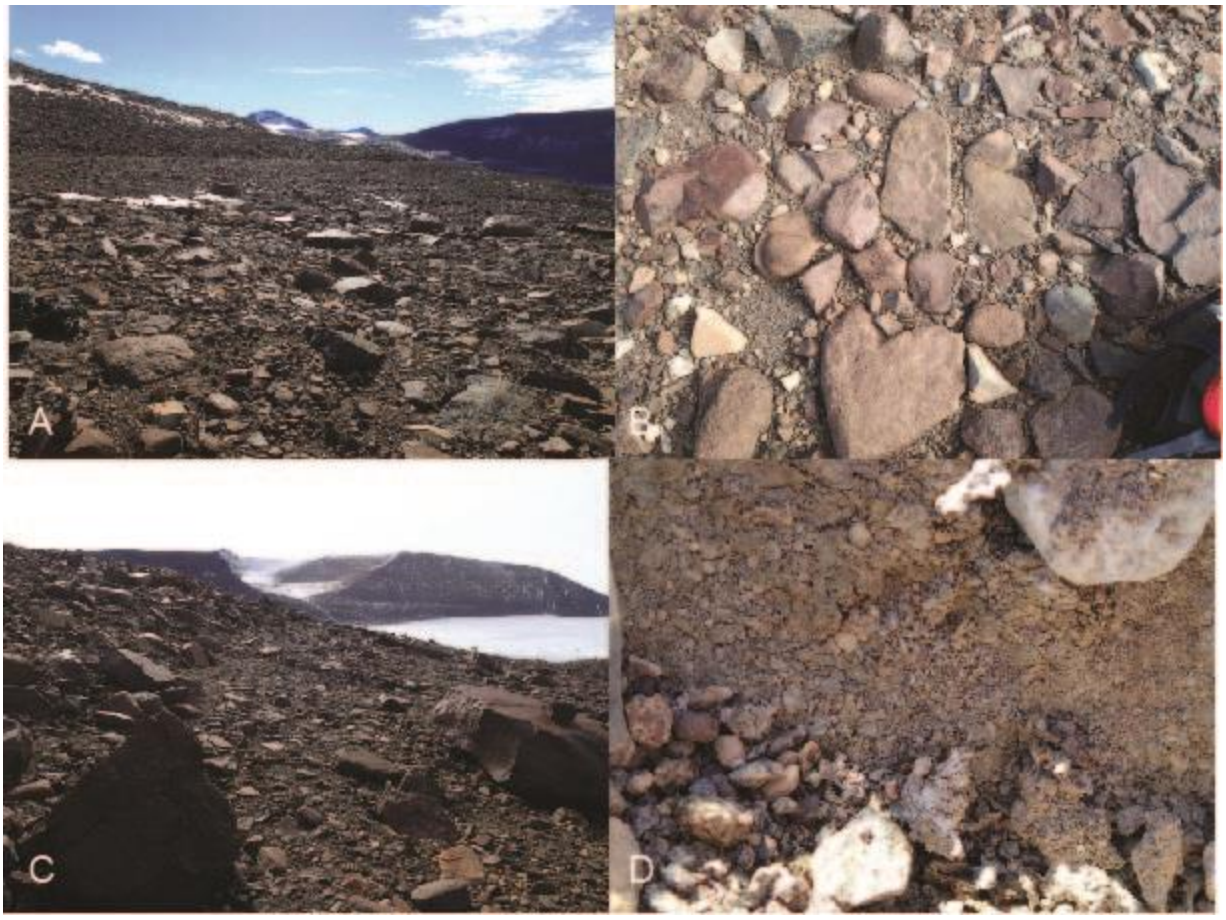

Figure S3. A. Shorelines etched into Britannia I drift in Lake Wellman valley. The lake that formed these shorelines must have been dammed by ice to the right of the photograph. B. Lake-ice boulder pavement. Nearshore areas of lakes in this region are characterized by interlocking, well-embedded boulders and cobbles. Cyanobacteria are abundant beneath these pavements. We propose that such pavements form in the moat zone where seasonal freezing leads to ice pressure on the lake-bottom clasts. C. Shoreline notch. Present-day Hatherton Glacier can be seen in the distance below to the right. The ice is ~150 m lower in elevation than the relict shoreline. D. Cyanobacterial mat preserved in sediments; field of view is ~20 cm.

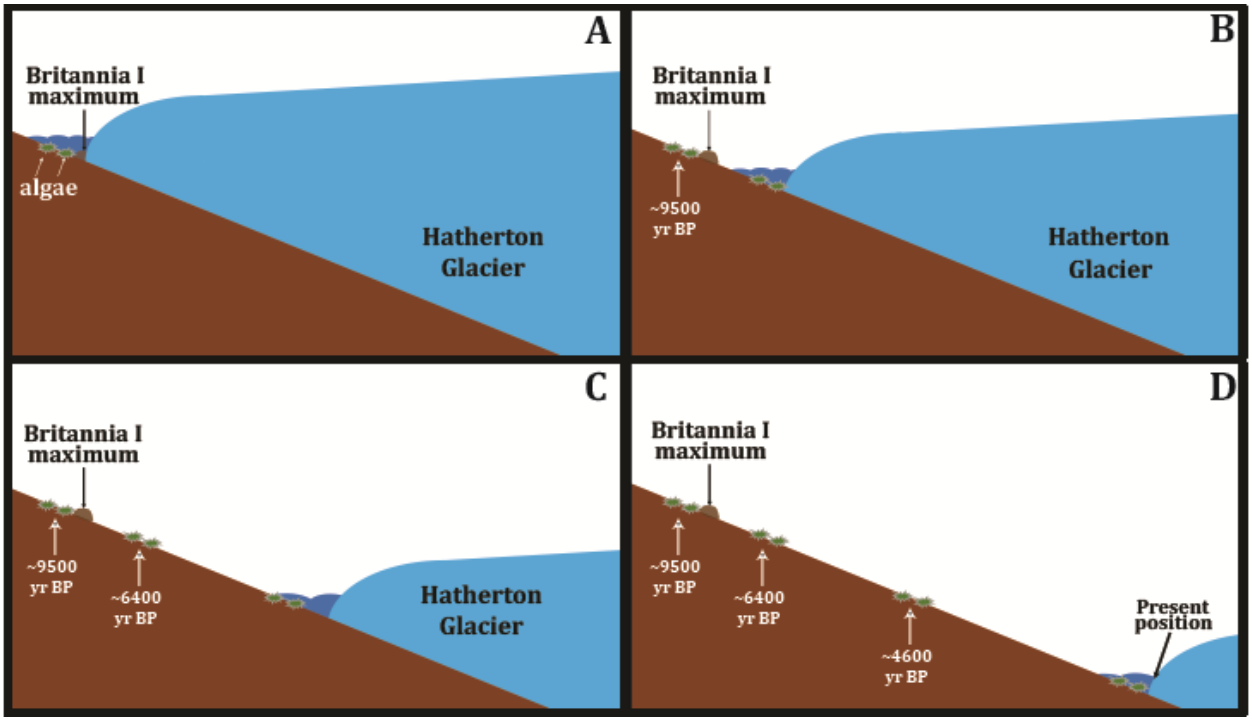

Figure S4. Schematic diagram of the relationship between the benthic cyanobacterial mats that grew in former ice-marginal lakes and past elevations of Hatherton Glacier for the Lake Wellman region. At the local LGM highstand, a lake was dammed against the margin of the glacier. Throughout recession, small, ice-marginal lakes followed the glacier terminus as it receded down the slope. Ancient cyanobacteria associated with these lakes, were stranded on the hillsides during this process and preserved in places beneath boulders and sediments. Radiocarbon ages become younger with decreasing elevation. The reverse process can occur during advance, although lacustrine sediments and associated cyanobacteria may be preserved in only select locations.

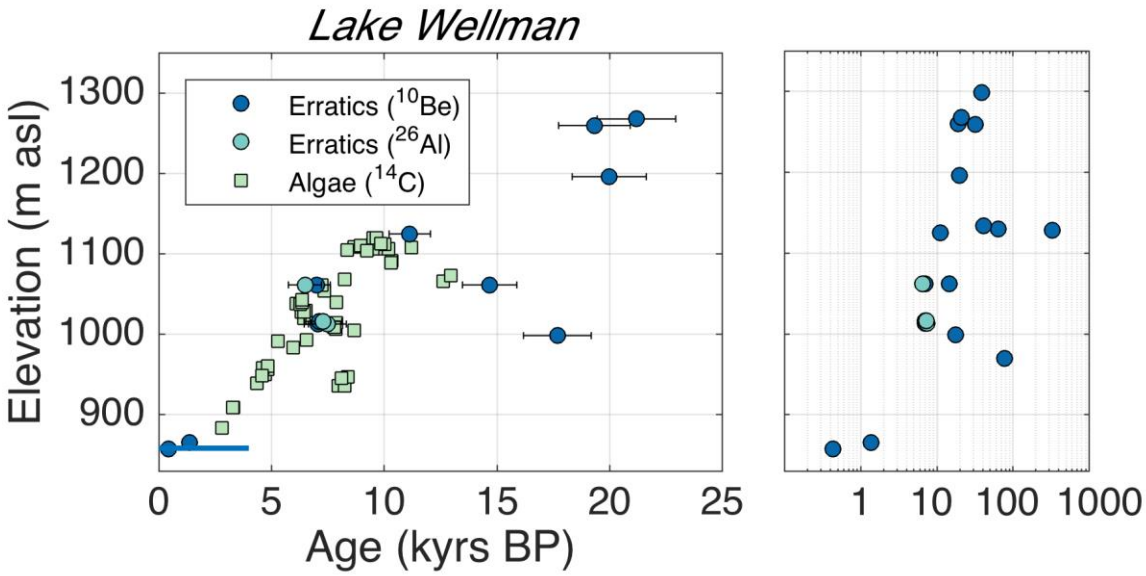

315

316 Figure S5. Age vs. elevation for both radiocarbon and cosmogenic isotope samples. The left
317 panel shows all ages and associated errors. The right panel shows only cosmogenic isotope
318 samples. Note the logarithmic scale. We caution that the age vs. elevation format provides only
319 one means of examining the data and does not account for significant elevation variation along
320 single limits that should yield internally consistent ages.

TABLE S1. RADIOCARBON DATA FOR SUBFOSSIL CYANOBACTERIA

No.	Lab Number	Latitude	Longitude	Elevation (m)	$\delta^{13}C$	^{14}C age (BP)	1σ	Cal. age (BP)	1σ
1	OS-117544	-79.89168	156.78500	1073	-2.34	11150	60	12980	140
2	OS-111165	-79.89144	156.78596	1066	-3.42	10650	60	12620	100
3	OS-111168	-79.89011	156.76419	1108	-1.25	9800	50	11220	70
4	OS-111166	-79.89112	156.77162	1091	-0.42	9210	40	10350	100
5	OS-117545	-79.89104	156.76873	1089	-0.87	9140	40	10320	90
6	OS-111167	-79.89045	156.76332	1106	-0.76	9040	40	10210	40
7	OS-117548	-79.89088	156.76346	1112	-0.58	8880	40	10030	150
8	OS-111155	-79.89091	156.75700	1113	-1.03	8840	40	9850	120
9	OS-110168	-79.89079	156.75648	1120	-1.75	8560	40	9520	40
10	OS-110170	-79.89064	156.76332	1106	-1.01	8680	55	9670	130
11	OS-111156	-79.89056	156.75764	1104	-5.06	8260	35	9230	100
12	OS-117509	-79.89080	156.76295	1110	-2.85	8070	50	8950	180
13	OS-117546	-79.89094	156.76283	1109	-4.64	7880	35	8690	100
14	OS-117512	-79.91129	156.79936	1005	-5.80	7860	50	8670	120
15	OS-117550	-79.91710	156.74017	947	-2.03	7600	35	8400	50
16	OS-117540	-79.88348	156.80006	1105	-3.79	7560	35	8370	40
17	OS-110174	-79.91720	156.75764	936	-2.38	7130	40	7970	50
18	OS-117637	-79.88631	156.81294	1068	-4.61	7480	120	8250	230
19	OS-117594	-79.91958	156.75159	945	-2.64	7320	35	8110	80
20	OS-111893	-79.91676	156.79649	1040	-8.03	7080	75	7880	150
21	OS-111160	-79.91089	156.80061	1014	-2.89	7040	40	7870	80
22	OS-111158	-79.91090	156.79849	1006	-4.33	7010	35	7850	90
23	OS-111161	-79.91168	156.79391	1009	-4.82	6980	30	7800	80
24	OS-111159	-79.91090	156.79787	1009	-5.33	6930	35	7760	80
25	OS-117542	-79.88738	156.81883	1054	-4.41	6410	30	7350	70
26	OS-117511	-79.88597	156.81592	1061	-3.33	6340	40	7250	80
27	OS-111169	-79.91355	156.80611	993	-4.32	5760	30	6570	80
28	OS-111916	-79.89040	156.80692	1029	-5.52	5740	100	6530	210
29	OS-111899	-79.89274	156.80466	1020	-5.20	5650	80	6440	140
30	OS-111157	-79.88879	156.81822	1028	-3.27	5640	30	6440	50
31	OS-117541	-79.88893	156.82394	1040	-3.54	5600	25	6360	50
32	OS-117543	-79.88792	156.81943	1043	-2.78	5600	25	6360	50
33	OS-117510	-79.89035	156.80685	1028	-2.97	5540	45	6340	70
34	OS-111900	-79.88846	156.82085	1037	-3.83	5460	65	6290	120
35	OS-111911	-79.88863	156.81898	1038	-4.72	5370	90	6120	180
36	OS-111163	-79.89536	156.81944	983	-6.47	5220	25	5960	40
37	OS-111164	-79.89556	156.81560	991	-6.58	4570	25	5300	20
38	OS-111162	-79.89645	156.82907	960	-2.99	4280	30	4850	30
39	OS-117513	-79.89735	156.82990	956	-2.61	4240	35	4840	30
40	OS-117507	-79.89759	156.83139	950	n.d.	4210	30	4730	40

No.	Lab Number	Latitude	Longitude	Elevation (m)	$\delta^{13}C$	^{14}C age (BP)	1σ	Cal. age (BP)	1σ
41	OS-117508	-79.89724	156.83049	958	-4.42	4110	30	4620	90
42	OS-117505	-79.89780	156.83310	948	-1.77	4090	30	4580	70
43	OS-117549	-79.89813	156.83624	939	-3.91	3920	20	4360	70
44	OS-110172	-79.91910	156.89320	909	-2.01	3110	30	3310	80
45	OS-117593	-79.89903	156.84862	883	-3.01	2720	20	2810	40

TABLE S2. METADATA FOR COSMOGENIC ISOTOPE SAMPLES

Sample	Latitude	Longitude	Elevation (m)	Thickness (cm)	Density (g/cm^3)	Shielding
13-HAT-004-LW	-79.92333	156.80100	1196	4	2.5	0.995338
13-HAT-006-LW	-79.92666	156.84691	1260	4	2.5	0.999572
13-HAT-007-LW	-79.92646	156.84644	1259	4	2.5	0.999549
13-HAT-009-LW	-79.91775	156.80047	1061	5	2.65	0.997257
13-HAT-010-LW	-79.9177	156.80041	1061	4	2.65	0.997506
13-HAT-018-LW	-79.91243	156.78796	1013	4.5	2.65	0.993860
13-HAT-020-LW	-79.91346	156.79340	1016	4	2.65	0.996814
13-HAT-029-LW	-79.89079	156.75929	1130	4	2.5	0.995794
13-HAT-030-LW	-79.89234	156.75795	1133	4	2.5	0.996208
13-HAT-031-LW	-79.89044	156.75995	1125	4	2.5	0.996517
13-HAT-036-LW	-79.91424	157.05614	1128	6	2.65	0.988984
13-HAT-041-LW	-79.91864	157.04753	998	5	2.5	0.996531
13-HAT-042-LW	-79.91943	157.04586	969	2	2.5	0.996962
13-HAT-044-LW	-79.93334	156.86501	1299	4	2.5	0.999266
13-HAT-047-LW	-79.92941	156.85678	1268	4	2.5	0.999203
13-HAT-049A-LW	-79.93291	156.96286	857	6	2.5	0.997605
13-HAT-058-LW	-79.91696	156.90154	865	6.75	2.65	0.998110

TABLE S3. CONCENTRATION DATA AND AGES FOR COSMOGENIC SAMPLES

Sample	^{10}Be (atoms/g)	1σ	^{10}Be age (years)	1σ	^{26}Al (atoms/g)	1σ	^{26}Al age (years)	1σ
13-HAT-004-LW	305,023	6498	19,996	428	0	0	n.d.	n.d.
13-HAT-006-LW	312,372	6651	19,340	414	0	0	n.d.	n.d.
13-HAT-007-LW	518,847	11,033	32,251	691	0	0	n.d.	n.d.
13-HAT-009-LW	198,651	4244	14,688	315	0	0	n.d.	n.d.
13-HAT-010-LW	95,881	3158	7017	231	620,306	26,774	6490	281
13-HAT-018-LW	91,769	2753	7056	212	680,958	28,420	7488	314
13-HAT-020-LW	93,477	2229	7118	170	669,309	31,824	7288	348
13-HAT-029-LW	926,219	19,609	64,893	1396	0	0	n.d.	n.d.
13-HAT-030-LW	603,135	10,616	41,867	745	0	0	n.d.	n.d.
13-HAT-031-LW	160,696	3547	11,145	247	0	0	n.d.	n.d.
13-HAT-036-LW	4,330,080	114,012	332,720	9531	0	0	n.d.	n.d.
13-HAT-041-LW	226,851	6874	17,693	538	0	0	n.d.	n.d.
13-HAT-042-LW	990,095	13,287	78,528	1075	0	0	n.d.	n.d.
13-HAT-044-LW	649,555	11,892	39,156	724	0	0	n.d.	n.d.
13-HAT-047-LW	344,478	7193	21,203	445	0	0	n.d.	n.d.
13-HAT-049A-LW	4900	506	433	45	0	0	n.d.	n.d.
13-HAT-058-LW	15,454	679	1368	60	0	0	n.d.	n.d.